Influence of irregularities in the rock underlayer on the stability of $Xbloc^{Plus}$

van den Berg, Ileen; Hofland, Bas; Reedijk, Bas

DOI
10.1016/j.coastaleng.2020.103637

Publication date
2020

Document Version
Accepted author manuscript

Published in
Coastal Engineering

Influence of irregularities in the rock underlayer on the stability of Xbloc$^{\mathrm{Plus}}$

Ileen van den Berg[a,c,*], Bas Hofland[a], Bas Reedijk[b]

[a] *Department of Civil Engineering, Delft University of Technology, Stevinweg 1, 2628 CN, Delft, The Netherlands*
[b] *Delta Marine Consultants, H.J. Nederhorststraat 1, 2800 AG, Gouda, The Netherlands*
[c] *DPI — Dutch Process Innovators, Suikersilo Oost 33, 1165 MS, Halfweg, The Netherlands*

Abstract

Many rubble mound breakwaters are nowadays made with an armour layer consisting of single layer interlocking elements. The stability of these armour layers could well be influenced by the irregularity of the rock underlayer, as that influences the degree of interlocking. Especially for the new types of regularly placed armour, this might be an important factor for the stability. However, this aspect has not been studied widely yet. Therefore, this paper investigates the influence of irregularities in the underlayer on the stability of a type of single layer breakwater elements. Model tests have been conducted in which the irregularities in the underlayer were systematically varied. The irregularities in the underlayer and the orientations of breakwater elements were measured with 3D-scanning. The breakwater armour unit used in the tests is the Xbloc$^{\mathrm{Plus}}$. A new failure mechanism, not previously observed for breakwater elements, was found to initiate damage. Causing the armour to be pushed outward by a combined effect of the weight of the upper armour

[*]Corresponding author; E-mail: i.vandenberg@dutchpi.com

and the excessive hydraulic pressure of the remaining water under the armour layer. Especially large-scale convex (i.e. protruding outwards) undulations in the cross-shore direction influenced the stability of the armour layer. This influence has been quantified.

Keywords: Breakwater, XblocPlus, armour layer stability, single-layer units, placement irregularity

1. Introduction

Background. Many rubble mound breakwaters are nowadays made with an armour layer consisting of concrete, single layer, interlocking elements. These armour layers obtain their stability not only from the weight of the single element on the slope, but also from interlocking and/or friction forces between the elements. Irregularities of the underlayer, typically made with randomly placed rocks of a smaller size, might influence the stability of the top layer of breakwater elements [Loman et al., 2012]. Still, to the authors knowledge, this aspect has hardly been studied. A logical explanation for the lack of in depth research in this area is the difficulty in finding a strong correlation between the underlayer configuration and the top layer stability. For randomly orientated elements not only the underlayer configuration influences the stability of the elements, but also the element orientation and placement densities [ten Oever et al., 2012]. Regularly placed elements such as the single layer cubes, Seabees and HARO's obtain their stability through lateral friction and are less sensitive for irregularities according to Van Gent and Luis [2013].

Recently however, new regularly placed elements such as the C-ROC [Perrin et al., 2017] and the Xbloc$^{\text{Plus}}$[Vos, 2017; Rada Mora, 2017] have been developed to facilitate the placement procedure. The elements are placed with both regular orientation and a regular placement grid, but obtain their stability due to interlocking instead of lateral friction. The regular placement reduces the fluctuations in element orientations and placement densities and emphasizes the influence of the underlayer configuration on the interlocking capacity and therefore the stability of the top layer. Especially since irregularities in the underlayer are the cause of fluctuations in placement densities and element orientations. At present, the tolerances for the underlayer used during the execution of breakwaters with single layer elements are mainly based on the experience in practice [Van der Zwicht, 2015] and are chosen such that the placement of the breakwater elements is facilitated. A detailed study on the influence on the stability lacks, such that the quantitative influence on the armour layer stability is unknown for any type of armour unit.

Aim. It is suspected that irregularities in the underlayer are important for the stability of regularly placed single layer elements. Hence this study focusses on the influence of the irregularity of the underlayer on the stability of the top layer. Possibly leading to guidelines for design criteria and construction tolerances.

We want to know how the stability of the armour layer is influenced by the size and direction of the distortions of the (otherwise straight) underlayer. The main parameters that are of importance to the stability will be identified and their influence will be quantified.

Approach. The element used during the research is the Xbloc$^{\text{Plus}}$, which is depicted in figure 1. Previous research on the element is used to provide insight in the mechanisms that are important for the stability of the element. The ongoing development programme of the new breakwater element Xbloc$^{\text{Plus}}$, provided an interesting opportunity for a study on the influence of the underlayer on their stability.

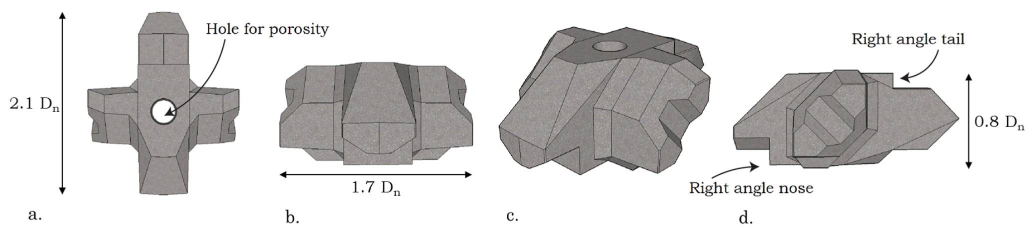

Figure 1: Shape of Xbloc$^{\text{Plus}}$, a) top view, b) front view, c) isometric view, d) side view

It is hypothesized that the stability of the elements decreases with decreasing radius of the distortions of the (otherwise straight) underlayer. Moreover, it is thought that the direction of the irregularities is of importance. These hypotheses were tested in 2D hydraulic model tests, where the irregularities were systematically varied, and the actual irregularities were measured in 3D. The results of the tests are used to validate the hypotheses and are further analysed to explain the observations. From the analysis follows the conclusion on how the stability is influenced and which aspects are of importance to predict the level of stability.

Outline. The evaluation of previous research on the element is found in the next section. Based on this knowledge hypotheses are formed (section 3) on which the test program and model set-up are based (section 4). In section 5 the processing of the 3D-data is explained, followed by the actual test results in section 6. The analysis is explicated in section 7, resulting in the discussion and conclusions.

2. Previous research

The Xbloc$^{\mathrm{Plus}}$ is an element that can be placed on straight, or in longitudinal direction slightly curved breakwater or revetment sections. The elements, shown in figure 1, are placed such that the same faces of the elements touch the elements underneath. Resulting in a regular placement, with both a uniform grid and an uniform orientation. The blocks are typically placed on a 3:4 slope.

Multiple modifications have been applied during the development of the Xbloc$^{\mathrm{Plus}}$. The results of the research performed on these earlier versions have gained insight in the influence of the modification and thereby on the aspects that are of importance for the stability of the element. The first version of the Xbloc$^{\mathrm{Plus}}$ was without the hole in the middle of the element and with chamfers instead of right angles at the nose and tail of the element (figure 1). The mechanism that governed the stability of this version was identified by Vos [2017]. The conclusion of the research was that failure occurred due to rotation of an element due to the drag during up-rush, after which extraction occurred as a result of uplift pressure on the armour layer (figure 2).

For the second version the hole was added to enlarge the porosity and reduce the uplift pressure. An increase in stability proved that the excessive uplift pressure is indeed a dominant factor for the stability. To improve the stability further, the interlocking capacity was enlarged by replacing the chamfers by right angles (figure 1). This improved the stability to such extent

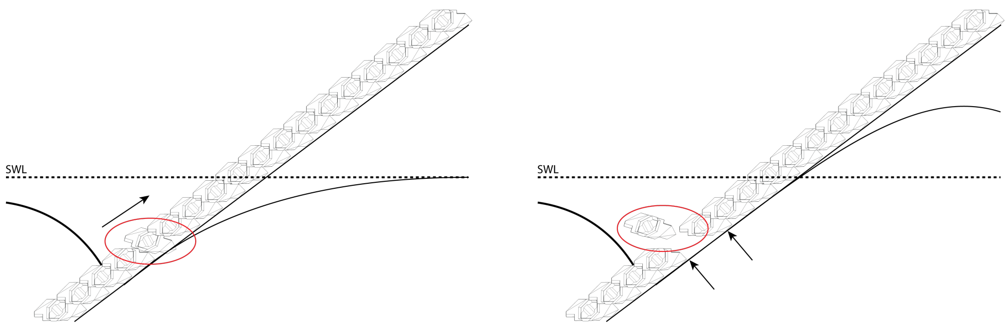

(a) Rotation of element due to up-rush

(b) Extraction of element due to uplift pressure

Figure 2: Failure mechanism for the first version of Xbloc$^{\mathrm{Plus}}$[Vos, 2017]

that failure no longer occurred at the tested scale and available wave facility. The maximum achieved stability number $\mathrm{N_s} = H_s/\Delta D_n$ was 4.0, where H_s is the incoming significant wave height, Δ the submerged dimensionless density, and D_n the nominal diameter of the element [Jacobs, 2017]. So the limit value of the stability number for this breakwater element was concluded to be higher than 4.0. Although it must be marked that these tests were done with a fixed toe and no safety margins have been included. As the tests were done with a straight, well-placed slope, the question arose how susceptible the element was to irregularities of the underlayer.

Several damage mechanisms have been identified for single layer breakwater elements [Garcia et al., 2013]. Rocking is not very important for the Xbloc$^{\mathrm{Plus}}$ as all elements are embedded. Since the replacement of the chamfers for the right angles, this phenomenon has only been observed directly before extraction. Also a displacement of the toe structure was seen to loosen the packing of several single layer armour types, which can lead to extraction of elements and failure of the armour layer [Hofland and van Gent, 2016]. This potential cause of damage was not tested yet for the Xbloc$^{\mathrm{Plus}}$.

It has been discussed before that the underlayer can influence the top layer stability for single layer (cubes) [Loman et al., 2012]. For the C-Roc block only the grading width of the underlayer was varied somewhat (M_{85}/M_{15} = 1.8 to 4.2, where M_{85} and M_{15} are the 85% and 15% percentiles of the grading curve of the underlayer rock). It was reported that this change of the underlayer did not noticeably change the stability of the top layer [Perrin et al., 2017].

Detailed 3D measurements of the toplayer surface of a Cubipod armour layer have been performed by Pardo et al. [2013]. The goal of this research was to measure the amount of randomness, which needed to be maximized for this particular breakwater element type, while the current research is focussed on small deviations from a regular pattern.

3. Hypotheses

The improved stability due to the introduction of the right angles at the nose and tail of the Xbloc$^{\text{Plus}}$ elements indicates the influence of interlocking on the level of stability. Therefore, it was expected that the amount of interlocking would be a key factor for the influence of irregularities in the underlayer on the stability of the Xbloc$^{\text{Plus}}$. Hence, theoretical relative angles between elements were determined for which the elements were no longer sufficiently interlocked and a significant drop of stability was expected. For the cross shore angles, the interlocking is lost when the right angle below the nose of the upper unit no longer hooks behind the lower unit. Long shore the interlocking was lost when the 'wings' of the elements were no longer supported by the two lower elements. The angles for which interlocking was lost were determined for each combination of shape (convex and concave) and direction (cross shore and long shore). These critical angles are indicated in Figure 3. An overview of the expected critical relative angles is given in Table 1.

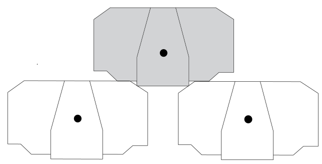

(a) Correct placement in x-direction (long shore)

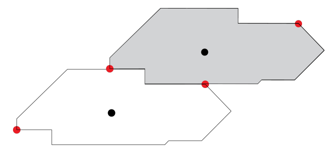

(b) Correct placement in y-direction (cross shore)

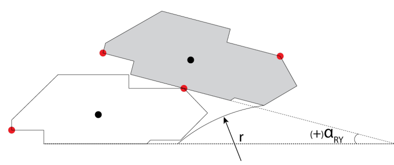

(c) Positive relative angle (convex) in y-direction (cross shore)

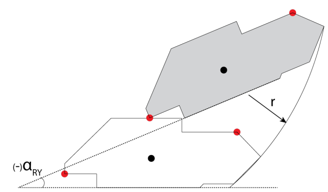

(d) Negative relative angle (concave) in y-direction (cross shore)

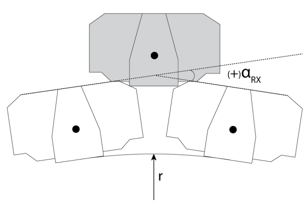

(e) Positive relative angle (convex) in x-direction (long shore)

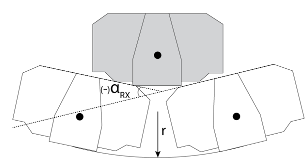

(f) Negative relative angle (concave) in x-direction (long shore)

Figure 3: Definitions of critical relative angles and radii, pertaining to upper (grey) elements in the figures

The shapes in long shore direction were expected to be the least critical, since these shapes only cause a distortion of the grid and no direct loss of interlocking. The initial rotation caused by a convex shape in cross shore

Direction	Shape configuration	Relative angle	Critical radius
Cross shore	Convex	(+) 23°	3.0 D_n
	Concave	(−) 15°	4.4 D_n
Long shore	Convex	(+) 38°	3.0 D_n
	Concave	(−) 18°	6.0 D_n

Table 1: Expected critical values

direction is similar to the rotation in the first stage leading to failure (figure 2a). Therefore, this configuration was expected to be critical. For a regular Xbloc, a convex (protruding), cross shore undulation was also seen to be the most influencing type of irregularity [Brouwer, 2013].

Next, these critical angles have been translated to the radius of curvature of the underlayer, for which these angles are expected to occur (also indicated in figure 3). It is hypothesized that this radius of curvature of the underlayer is of influence on the stability of the layer, and that a strong decrease of stability occurs if the occurring curvature becomes smaller than these critical curvatures.

The previously determined hypotheses were also expected to be valid for more realistic configurations. Relevant realistic configurations are micro-irregularities with length scales of several diameters of the rock of the underlayer (see figure 4a) and S-profiles [Van der Meer, 1988] that can be present in the underlayer due to small storms during construction (figure 4b).

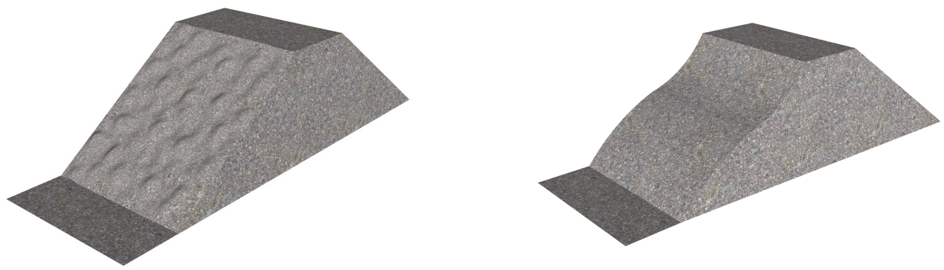

(a) Impression micro irregularities

(b) Impression S-profile

Figure 4: More realistic irregularities

4. Model set-up

The influence of irregularities on the stability of the $\text{Xbloc}^{\text{Plus}}$ is determined by performing physical model tests. The cross section of the tested structure is depicted in figure 5.

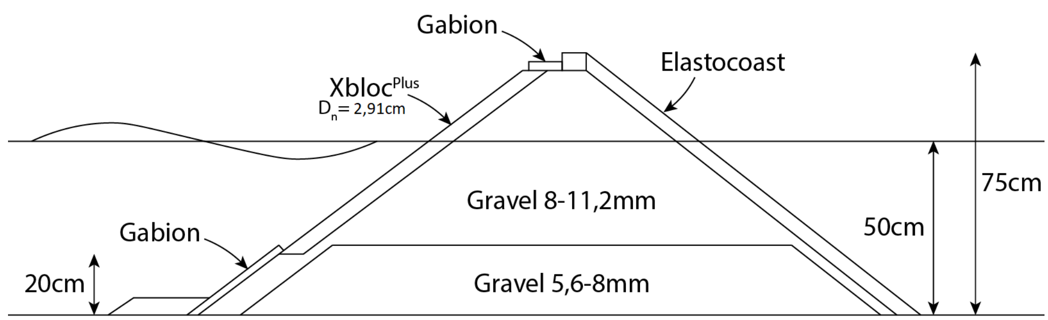

Figure 5: Cross section of the model structure geometry

The tests are performed with a slope of 3:4 because a steep slope is expected to be more conservative with regards to the stability [Angremond et al., 2008]. The freeboard was chosen to be 2.5 times the $H_{s,design}$. $H_{s,design}$ is the design wave height chosen by block developers Delta Marine Consultants as the wave height that leads to a conservatively stable stability number of 2.5. The maximum tested H_s is 1.5 times this $H_{s,design}$. Resulting in relatively few waves reaching the crest of the structure. This was chosen such because the stability of the crest is not an objective of this research.

The model elements had a D_n of 2.91cm, a relative density of 1.36 g/l, a width of 4.88cm, a height of 2.44cm, and a length of 6.19cm. The Reynolds number ($\sqrt{\mathrm{gH_{s,design}}}D_\mathrm{n}/\nu$) is below $3 \cdot 10^4$ and therefore underneath the limit where non-developed turbulent flow inside the porous medium starts to influence the stability of the top layer [Dai and Kamel, 1969].

The guideline of DMC for the W_{50} ratio between the underlayer and breakwater elements is between 1/10 and 1/20. The underlayer and core are of the same grading to prevent deviations in thickness of the underlayer, that could influence the results by causing a varying porosity. The combined core and underlayer is chosen to be of the standard grading of 8-11.2mm, which gives a W_{50} of $\approx$1/20.

The crest and toe are outside the scope of this study and built with a higher stability than expected in reality to prevent failure at these locations. The target fictitious deep water wave steepness was $\mathrm{s_{op}}$=0.04. Which is a commonly used wave steepness to represent wind waves in design storms [Angremond et al., 2008].

The model tests are conducted in the wave flume of Delta Marine Consultants in Utrecht, the Netherlands. This flume is 60cm wide, 100cm high and has a length of 25m. All tests are performed with a constant water depth of 50cm and without a foreshore to prevent breaking of the waves before the structure is reached. The maximum applied wave height is $\mathrm{H_s}$ = 16cm. The waves are irregular based on a JONSWAP-spectrum with γ=3.3 and each test consists out of 1000 waves. The flume has a piston-type wave board with an Active Reflection Compensation system, which damps out the reflected waves.

Test program. The total test program is subdivided into seven test-sections, each test-section is testing a specific type of irregularity and consists out of various test series. All test series are conducted with different sizes and/or locations of the type of irregularity. In total 26 test series have been performed, with a total of 177 test runs. Each test series consisted of two to six separate test runs with stepwise increasing wave height by 20% or 10% until damage occurred, or until the limit of the wavemaker was reached. Some representative conditions of the various test runs are given in table 2

Test run	H_s	T_p	N_s	$\frac{H_{0.1\%}}{H_s}$
1	0.0639	0.99	1.6	1.94
2	0.0834	1.14	2.1	1.93
3	0.102	1.29	2.6	1.85
4	0.122	1.40	3.1	1.77
5	0.132	1.42	3.3	1.62
6	0.138	1.55	3.5	1.73
7	0.146	1.58	3.7	1.56
8	0.154	1.57	3.9	1.52

Table 2: Representative test conditions per run

Out of the 26 test series, only 11 series resulted in failure. This limits the certainty of when exactly failure will occur. However, the tests without failure do yield a conservative lower bound for the critical damage number.

The test program is divided in three separate parts. Part I consists of test-section 1, and has the goal to determine the stability without any intentional irregularities. It is the reference case to which the other test-sections can be compared to and the effect of the irregularities is determined with. Part II covers test-sections 2 up to 5, which are the series with macro irregularities in different directions and shapes. The goal of this part of the test program is to either validate or disprove the stated hypotheses. In part III, the final part of the test program, more realistic configurations are tested. Part III comprises test-sections 6 and 7.

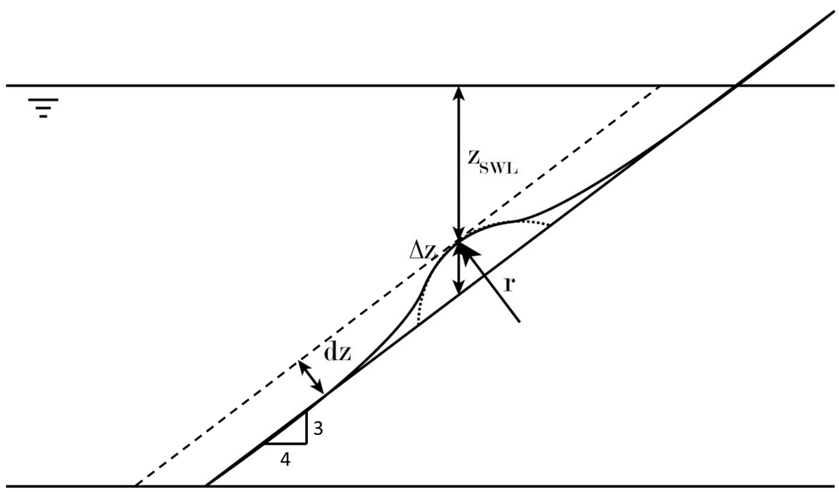

Figure 6: Aspects relevant for target size and location

For part II, each series within the test-section has a different size and/or location of the specific type of irregularity. An overview of all the different series and their specific irregularities is given in Table 3. The target values for the size and location of the irregularities is also given in this table. The target value for the radius of the irregularity is given relative to the hypothetical critical radius. The maximum vertical deviation from the design profile is given as Δz. The location of the irregularity along the profile is given relative to the Still Water Level, indicated by z_{SWL}. Both values are given relative to the breakwater element size (D_n). Figure 6 shows the geometrical notations.

		Irregularity type			Target size and location				
Part	Section	Direction	Shape	Series	$\frac{r}{r_{hyp}}$	$\frac{dz}{D_n}$	$\frac{z_{SWL}}{D_n}$	# Runs	$N_{s,max}$
I	1	N.a.	Straight slope	1	n.a.	n.a.	n.a.	8	> 3.9
II	2	Cross shore	Convex	1	1.0	1.0	-3.4	5	3.3
				2	1.2	1.0	-3.4	8	> 3.9
				3	0.8	1.0	-3.4	2	2.0
				4	1.0	0.8	-3.4	7	3.8
				5	1.0	1.0	0.0	8	> 4.1
	3	Cross shore	Concave	1	1.0	1.0	0.0	8	> 4.2
				2	0.8	1.0	0.0	8	> 3.9
				3	1.0	1.0	-3.4	7	3.7
				4	1.0	1.0	-1.7	8	> 3.9
	4	Long shore	Convex	1	1.0	1.0	n.a.	8	> 3.9
				2	1.2	1.0	n.a.	8	> 4.0
	5	Long shore	Concave	1	1.0	1.0	n.a.	8	> 3.9
				2	1.0	1.0	n.a.	8	> 4.2
				3	0.8	1.0	n.a.	8	> 4.0

Table 3: Overview test configurations, part I and II

In part III the irregularities are present over the full length and width of the test area. In test-section 6 the irregularities are randomly applied, therefore the sizes are not specific but an estimated value. The values are given in table 4. The S-profile configurations in test-section 7, are made by applying a certain $H_s/\Delta D_n$ to the underlayer. D_n is the nominal model element diameter of the side of the volume equivalent cube, which is approximately 20 times the D_{n50} of the underlayer. Multiple tests have been done with different wave heights and durations of application, an overview of the differences is given in table 5. If another size of underlayer is used than was used for the present tests, or if different wave heights occur during construction, different S-profiles can occur in the under layers. Hence the size of the irregularity (dz) is used as the parameter to quantify the influence of the irregularity on the block stability.

Part	Section	Irregularity type: Direction	Irregularity type: Shape	Series	Target size: Below SWL $\left[\frac{dz}{D_n}\right]$	Target size: Above SWL $\left[\frac{dz}{D_n}\right]$	# Runs	$N_{s,max}$
III	6	All	Micro irregularities (figure 4a)	1	1.0	1.0	8	> 4.0
				2	1.1	1.1	8	> 3.9
				3	1.2	1.2	8	3.7
				4	1.2	1.0	6	3.1
				5	0.8	0.8	8	> 3.9

Table 4: Overview test configurations, part III test-section 6

Part	Section	Irregularity type: Direction	Irregularity type: Shape	Series	Applied waves: $\frac{H_s}{\Delta D_n}$	Applied waves: Duration [min]	# Runs	$N_{s,max}$
III	7	Cross shore	S-profiles (figure 4b)	1	1.5	≈ 7	3	2.6
				2	1.5	≈ 2	8	> 3.9
				3	1.5	≈ 5	3	2.5
				4	1.0	≈ 10	6	3.5
				5	1.3	≈ 10	6	3.7
				6	1.4	≈ 10	4	3.1

Table 5: Overview of test configurations, part III test-section 7

The number of series within each test-section was not known beforehand and is based on the output of the previous tests. The goal is to obtain the stability parameter for different sizes of the irregularities, so a critical value can be determined. If failure occurs during an early run, the next test is performed with an irregularity of a smaller size. Vice versa, the irregularity is increased when failure occurs at high wave heights or not at all. The irregularity is not increased beyond the boundaries of what would be realistic in practice. In that case the test program is continued with the next test-section.

5. Digital Elevation Model processing

The angle of the elements relative to its neighbouring elements is considered to be the aspect of interest. Therefore, the orientations of all elements in the test section needed to be measured. The orientations were obtained from a Digital Elevation Model (DEM). This DEM was obtained from a point cloud that was created with Autodesk ReCap, based on about 50 photos made by a Huawei P9lite 13 Mpix mobile phone camera. The conversion from 3D-point clouds to DEM and subsequent processing was done in Python.

Each test configuration was measured both at the beginning of the test series and after the last test was performed. At these moments the configuration of both the underlayer and the armour layer were measured, unless the damage after the test runs was too severe for the model to be meaningful. At the beginning of each test two sets of 40-60 photos were made, from which three models were created. One model of each photo set and one model of (a random selection of) the combined photo sets. The multiple DEM's enable us to estimate the accuracy of the recordings, and averaging over the three models reduces the random errors. At the end of the test series only one set of photos was taken.

The ReCap program calculates a point cloud from the set of photos, which is shown in figure 7. The point clouds have 41000 to 45000 points in the region of interest. From the point cloud the points in the test section are extracted. For each point the x,y,z-coordinates and the RGB color values are determined. The z-axis is defined upward from the bottom of the flume, the y-axis in the length of the flume and the x-axis over the width of the flume with its origin at the left side of the flume (facing the slope). All the

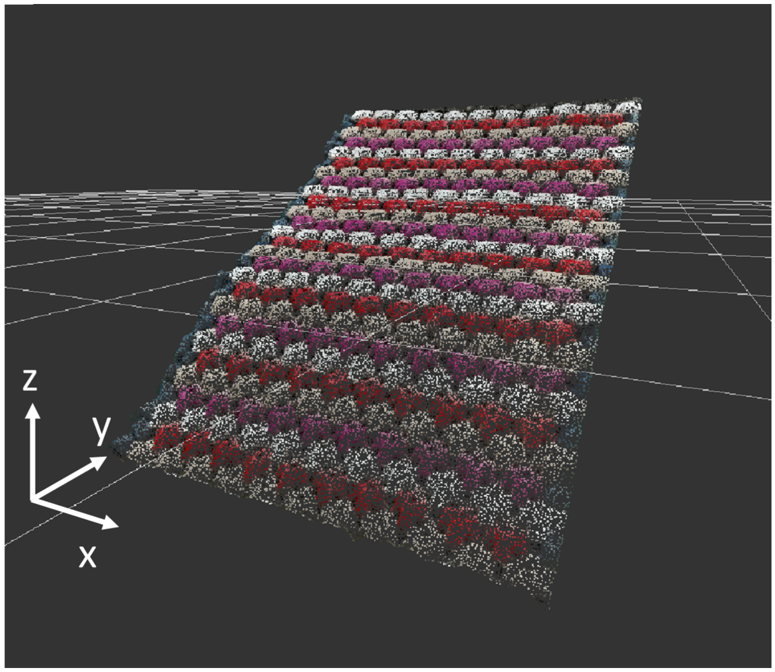

Figure 7: Example ReCap point cloud

models are fixed in the same axial system by using four fixed targets. Two on each side of the wave flume, one at the level of the crest and one just above the first row of breakwater elements. Each target of each model is selected manually in ReCap. To reduce errors in the target registration the zoom function of the program was used and each target has been selected on at least eight pictures.

The point cloud is loaded into Python and reinterpolated onto a regular x,y-grid for further processing, resulting in a DEM with a grid spacing of 0.00025m.

Next, the separate elements need to be identified. With the x,y-coordinates and the colour values a top view is compiled from which the element locations are determined with the MatchTemplate routine by OpenCV [Docs.opencv.org]. The element locations are checked visually during processing, in both the compiled top view and the plot of the z-coordinates relative to the straight target profile (without irregularity). Figure 8 shows an example of these top views of the DEM of a test series 1 from section 2 (convex in cross shore direction) with indications of the automatically identified locations of the elements.

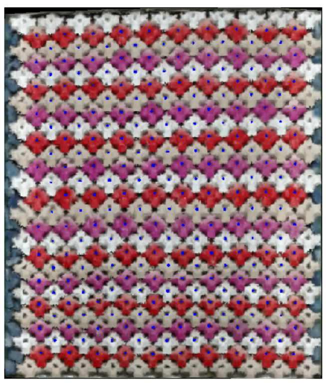

(a) Compiled top view with element locations

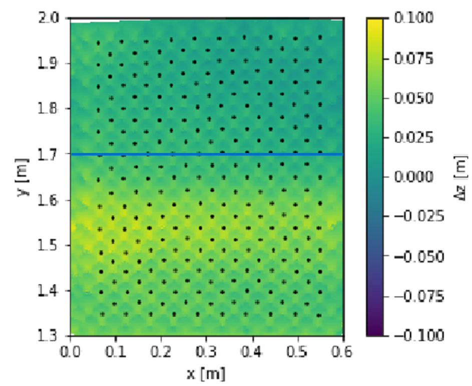

(b) Plot 3D-coordinates with element locations

Figure 8: Check of element locations of section 2 (convex in cross section) test series 1

The orientation of the top of the element is determined in x and y direction at the element locations and recalculated into angles. To prevent small measurement errors from affecting the result, the slope is averaged over a square area of 25mm^2 in the x,y-plane, around the centre of mass of the element. This area was chosen as a compromise between cancelling out model noise and preventing errors due to inaccuracy of the element locations.

The corresponding orientation of the underlayer at the element locations are measured as well. This is measured at the location were the tail of

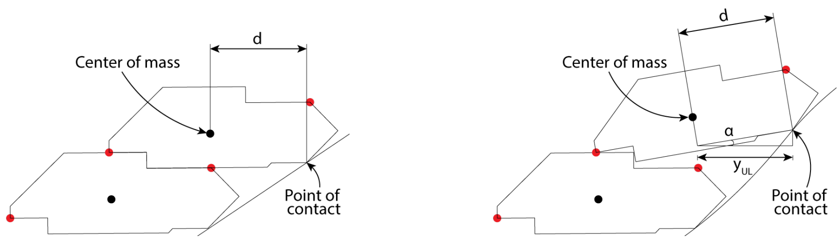

(a) Distance d, between found location at center of mass and contact point with underlayer

(b) Angle of element with orientation of element taken into account

Figure 9: Calculating corresponding location underlayer

the breakwater element contacts the underlayer, as is depicted in figure 9. To prevent single grains from affecting the slope of the profile, the DEM is smoothed with a Gaussian filter with a standard deviation equal to the D_{n50} of the underlayer. The result of smoothing is depicted in figure10, in which indeed it can be seen that the individual grains are smoothed out while the larger profile deviations are maintained.

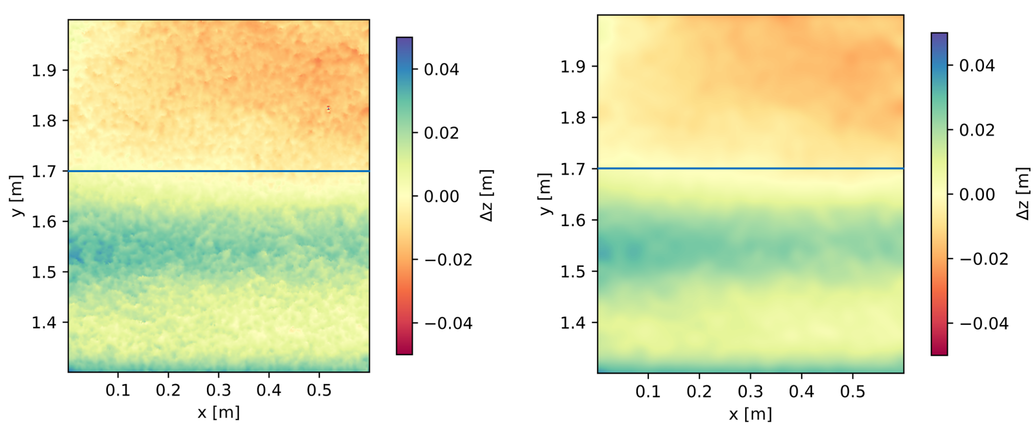

(a) Deviation from design profile

(b) Result after smoothing

Figure 10: Effect from electronic smoothing of underlayer test series 1 section 2 (convex in cross section)

Further reduction of measurement errors is accomplished by averaging the angles of each location over the three models that have been made at the same moment. After averaging, the relative angles are calculated.

In y-direction the relative angle (α_{RY}) is calculated as the angle of the element minus the average angle of the two supporting elements underneath. In x-direction the relative angle (α_{RX}) depends on the two elements underneath, it is calculated as the angle between the two elements. The exact definitions of the positive and negative relative angles for both directions is visualised in figure 3.

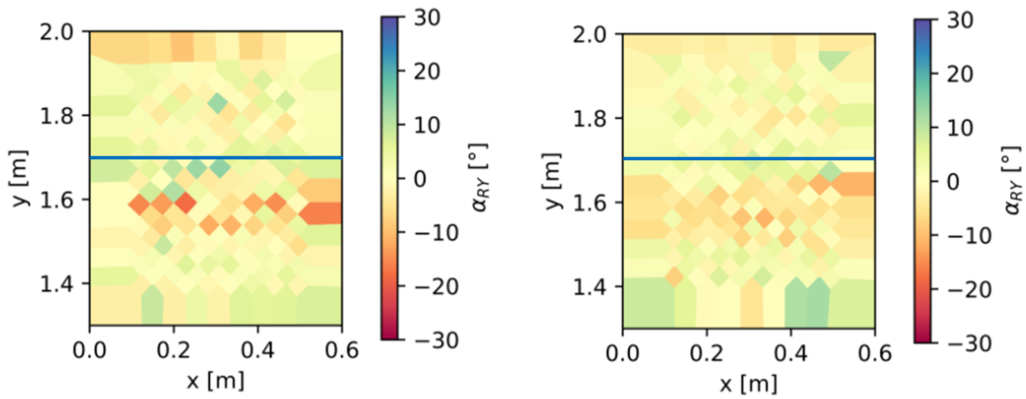

(a) Armour layer (b) Underlayer

Figure 11: Calculated relative angles of section 2 (convex in cross section) test series 1

The results of the relative angles for the same case are visualised at the locations of the elements as in figure 11. These fields with relative angles have been created for all test series.

For all test series, the relative angles are extracted for the breakwater element where failure occurred and related to the N_s for which the failure occurred. If no failure occurred the maximum measured values of α_R and

N_s are taken. This constitutes the final information that is used for further analysis. The same is done with the relative angle of the corresponding underlayer.

The three ReCap models made at the same moment are compared to indicate the accuracy of the data. For each test series the three models have been compared to the average of the three models combined.

The average standard deviation of each point over the three models is less than 1mm. The maximum deviation between the models is 5mm. This maximum deviation however, occurs at the transition between elements. At the top of the element, where the data for the element orientation is extracted, the maximum deviation is 3mm. For the underlayer there are exceptions where the deviation is 5mm, most models have a maximum deviation of 3mm. The calculated angles have an average standard deviation of 2.2° for the armour layer and 0.4° for the underlayer in both x- and y-direction. The errors are expected to be random and to be further reduced by averaging over the three models.

6. Test results

All tests were executed according to plan. In many test series, no extraction of units could be obtained for the top layer with the capabilities of the wave facility. In these series it could only be concluded that $H_s/\Delta D_n > 4$.

The hypothesis are based on the assumption that the orientation of the breakwater elements is influenced by the condition of the underlayer. In Figure 12 an example is shown of the S-profiles where it can be seen that the measured angles of the underlayer indeed correspond to the measured angles of the element orientations.

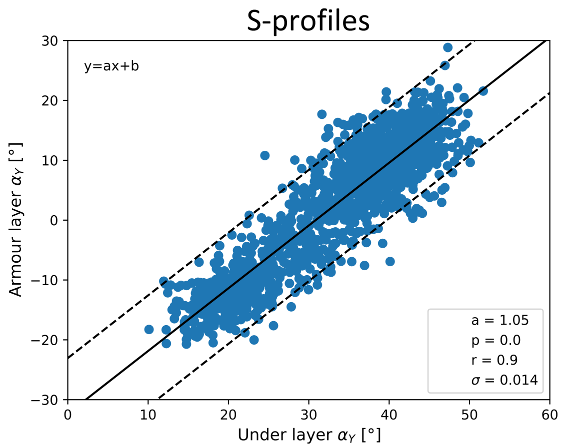

Figure 12: Correlation between angles measured for S-profile tests in underlayer and amour layer

The convex shape in cross shore direction resulted to be, as expected in the hypotheses, the most critical configuration. This was the only shape for which failure occurred during the test program. For the other shapes and directions no failure occurred and these tests are thus not further discussed in this paper. Also in Part III of the test program, failure occurred only at the areas with a convex shape in cross shore direction. The measured relative angle of the failed elements are related to the N_s for which failure occurred. The preceding tests without failure are given for reference in Figure 13.

For both the armour and underlayer a large spreading can be seen in the results and no clear dependency between α_{RY} and $H_s/\Delta D_n$ can be derived. The measured relative angles of the underlayer are smaller than the resulting angles of the elements. This is expected to be an effect of the smoothing applied to the measured underlayer.

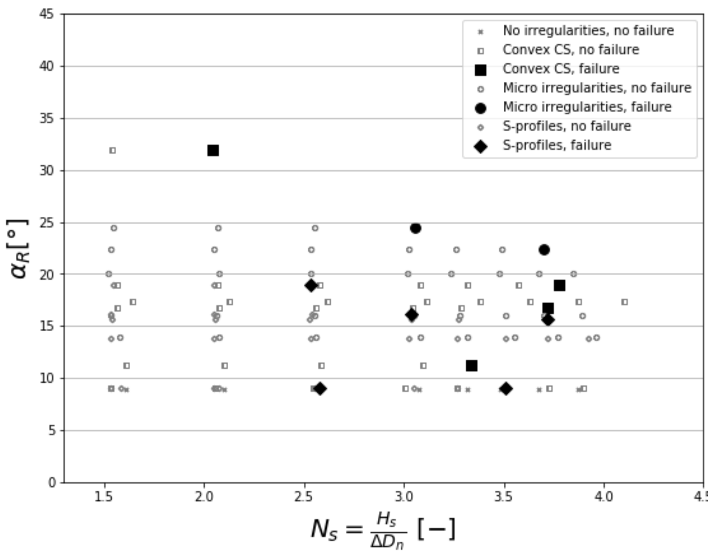

(a) Armour layer

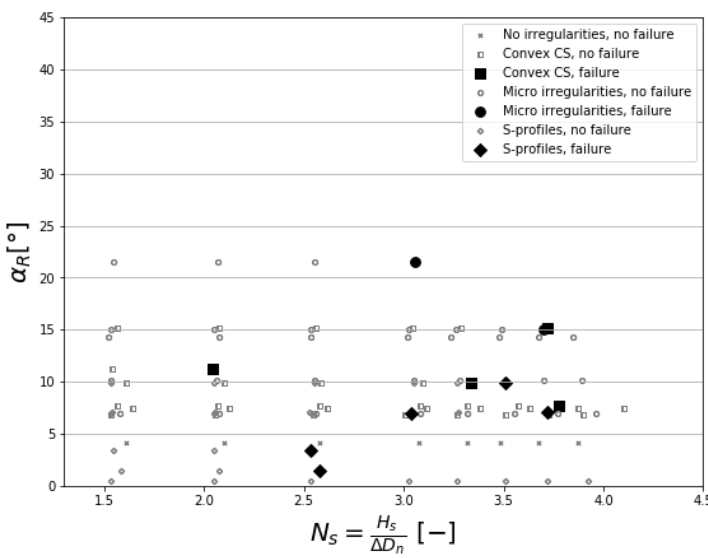

(b) Corresponding underlayer

Figure 13: Correlation $\mathrm{N_s}$ and α_R; black markers indicate failure

It is observed during the tests and from the test results that test series with approximately the same relative angles had an earlier failure when the

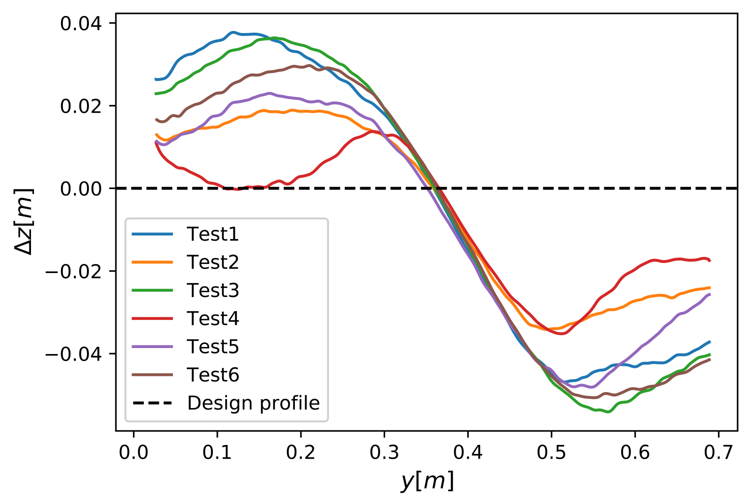

Figure 14: Measured deviations of the underlayer from the design profile of the S-profiles in test section 7

deviation from the design profile was larger. An example of the differences in deviation from the design profile is given in Figure 14.

Additionally, it was observed during the tests that, especially during sudden failure, the lower part of the slope moved away from the slope and the upper part moved downward. This was also seen in the measurements of the vertical differences between the start and end of the test series, as well for test series that failed as for test series where no failure occurred (Figure 15).

7. Analysis

The large spreading in the test results indicated that the relative angles between neighbouring elements are not the only factor of influence. It was seen that configurations with approximately the same relative angle (α_R) but a larger deviation from the design profile resulted in earlier failure. Which led

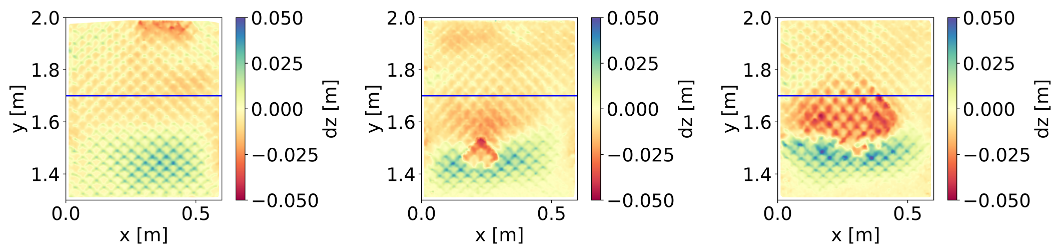

(a) Section 2, test series 2 (convex shape)

(b) Section 7, test series 5 (S-profile)

(c) Section 7, test series 6 (S-profile)

Figure 15: Measured difference in vertical elevation of the armour layer between start and end of test series

to the expectation that the deviation from the design profile influences the stability as well. The results showed that more specifically the steepness of the lower part of the convex shape is a good indicator of the influence on the stability. For many types of elements, a steeper slope decreases the strength of the top layer [Hudson, 1959]. Subsequently, this steepness is influenced by both the absolute deviation from the design profile and the length over which the deviation occurs. This is expressed in the additional parameter β, which is the average additional angle resulting from the deviation from the design profile. Measured as the angle resulting from the length (L1) between the lower edge of the protrusion ($\Delta z' \approx 0$) and the top of the convex shape and the difference at the top of the convex shape between the measured profile and the design profile, as is visualised in Figure 16.

Parameter β is considered to be zero for the (small scale) micro irregularities. With this assumption taken into account, empirical results showed that the summation of α_R and β results in a significant reduction of the spreading in the results as can be seen in Figure 17.

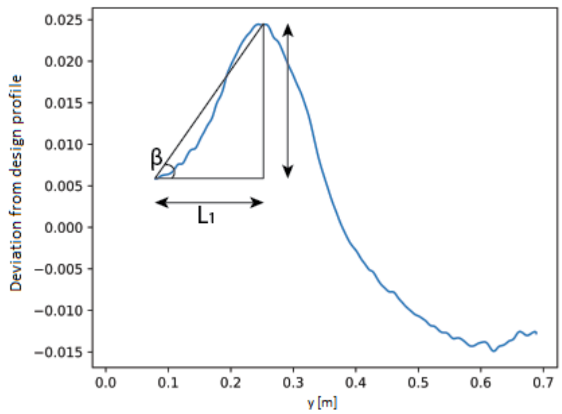

Figure 16: Visualisation β

The resulting trend line of the armour layer is given by equation 1. The trend line of the corresponding underlayer is given by equation 2.

$$Armour\ layer:\ N_s = -0.1(\alpha_R + \beta) + 5.7 \tag{1}$$

$$Underlayer:\ N_s = -0.3(\alpha_R + \beta) + 8.2 \tag{2}$$

The influence of β on the stability of the profile can be explained on the basis of an extremely simplified model. The model is based on the S-profiles since the influence of β was seen best during testing in these profiles.

In the model the elements above and underneath the top of the convex shape are considered to be two rigid bodies. Thus assuming that the elements inside the rigid bodies are fully interlocked. The lower rigid body is fixed with a hinge at the lower edge of the protrusion and linked with a hinge to the upper rigid body. The upper rigid body is considered to be connected to the design profile with a roller bearing by means of a hinge. The schematisation

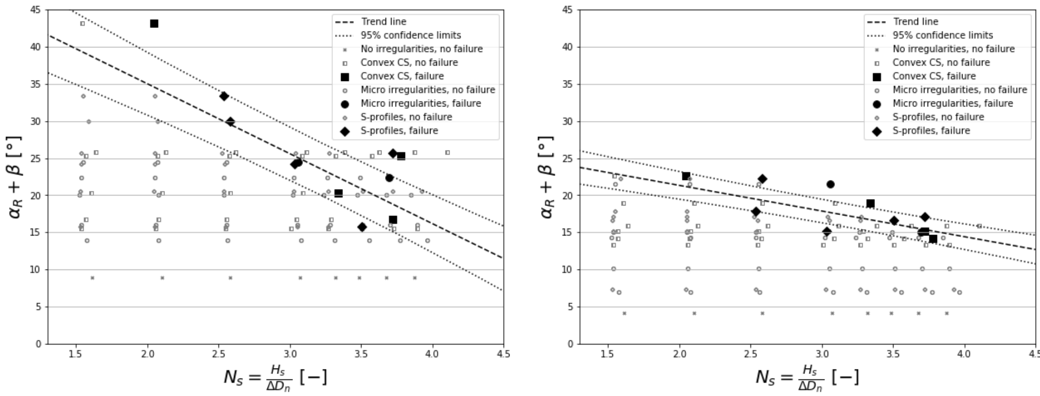

(a) Armour layer (b) Corresponding underlayer

Figure 17: Correlation $\mathrm{N_s}$ and $\alpha_R + \beta$

and visualisation of the simplified model is given is Figure 18.

The up- and down-rush of the waves takes place along the upper rigid body. The most critical moment is considered to be during maximum run-down. Assumed is that the gravity force of the upper rigid body is then fully counteracted by the pressure force underneath the body. The only modelled force on this body is the effective drag force ($\mathrm{Fd_{eff}}$). The effective drag force is the drag force, complemented by the weight of the elements above the convex section, minus the friction of the underlayer. This force causes a rotation of both the rigid bodies resulting in an enlarged relative angle. The only modelled force on the lower rigid body is the gravity force. This is the resistive force against the movement of the rigid bodies.

The angles α_R and β are dependent of each other, this relation can be described by the following formula.

$$\alpha_R \approx \beta \left(1 + \frac{L_1}{L_2}\right) \tag{3}$$

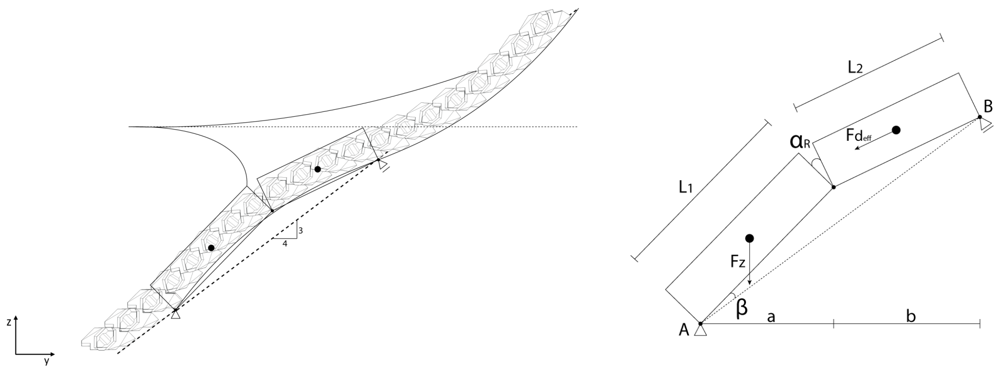

(a) Schematised S-profile

(b) Simplified model

Figure 18: Schematisation of S-profile into simplified model

An increase of β results a reduction of the leverage arm of the resistive force around point A. Thereby reducing the resistance against rotation of the rigid bodies. An increase of α_R enlarges the leverage arm of the acting force ($\mathrm{Fd}_{\mathrm{eff}}$) around point A and induces the rotation of the rigid bodies. Thereby explaining the influence of these parameters on the stability. If the resistive moment is smaller than the acting moment, the rigid bodies are lifted away from the underlayer. Resulting in an enlargement of the convex shape and α_R, ultimately causing failure.

The movements indicated by the simplified model, have been measured in the tests. For tests both with and without element extraction, as can be seen in Figure 15. The movements seen in the measurements however slightly deviate from the movements indicated by the simplified model. Since the upper rigid body fully subsides in the simplified model instead of only partially, as can be seen in the measurements. This difference could be due to the fault that the model does not take the movements of the underlayer into account. When the lower elements move away from the underlayer, the underlayer is no longer stable and the grains will move downward. Which causes the upper rigid body to subside.

The analysis indicates that the relative angle between the elements at the top of the convex shape (α_R) determines whether it is possible for the element to be extracted from the profile. The steepness (β) of the slope downward from this point however, can cause an enlargement of (α_R) and therefore influences the level of stability as well.

8. Discussion

The wavemaker is piston-type, a rule-of-thumb for the maximum generated waves in a given water depth is around half the water depth, i.e. 0.25m. The maximum applied wave height is $\mathrm{H_s}$ = 0.16m, assuming Rayleigh distribution and 1000 waves, the maximum wave height should be around 0.31 m. This means that the maximum waves in the extreme sea state will break near the wavemaker, so the wave height distribution is trimmed in the upper tail. This is one of the possible reasons the maximum waves in the sea states were not achieved (see table 2) and as a consequence, initiation of damage was not reached in most of the test series carried out.

The radii of the hypothetical critical irregularities in cross shore direction were much smaller than the length of the profile. This introduces an additional parameter that is of influence for the damage: the position of the irregularity ($\mathrm{z_{SWL}}$, see figure 6). Research on a previous version of the XblocPlus showed that the expected location of damage (initial extractions) occurred between 1.0 and 1.5 Hs below the still waterline [Rada Mora, 2017]. Most effect of the irregularity could then reasonably be expected with the irregularity placed around that depth. The irregularities were mostly placed at a depth of 3.4 D_n. Thus, for a typical stability number $H_s/(\Delta D_n)$ of 2.5, the irregularity was placed at roughly 1 H_s under the water line, and for the maximum stability number of 4.0, the top of the irregularity was placed at 0.5 H_s. Therefore the irregularity was placed around the location of highest wave attack, but possibly somewhat high for the tests with the largest wave heights. The obtained test results confirm the influence of the depth of the irregularity, since for example in series 5 of section 2 a higher placed irregularity resulted in less damage.

As stated above, initial extractions of units typically occurred between 1.0 and 1.5 H_s below the water line [Rada Mora, 2017]. This damage location around the rundown point of the waves is remarkable, as for typical rubble mound (rock) slopes initial extraction often occurs around the water line, where flow velocities are highest [De Almeida et al., 2019]. This location could indicate that for this rather impermeable top layer, the damage is (partly or largely) induced by excessive water pressures under the armour layer during rundown of the wave, as occurs for placed-block revetments [CUR, 1995].

The D_{n50} of both the core and underlayer are of the same size and gradation. This choice has been made to prevent the thickness of the underlayer to influence the results by introducing a variable permeability. Both the D_{n50} and gradation have been chosen relatively small. The small element size is expected to give a conservative result with respect to the stability [Burcharth and Andersen, 1995] and the grading is expected to have no significant influence [Perrin et al., 2017].

The toe of the tested model was fixed and thus too stable in relation to what would be designed in practice. At the locations where the armour layer was located on a protruding (convex) irregularity under the mean water line damage occurred during wave rundown. The armour layer at this location was pushed outward by a combined effect of the weight of the upper armour and the excessive hydraulic pressure of the remaining water under the armour layer. This is less likely to occur with a toe structure that is barely sufficient. Failure could then occur due to sliding of the toe, causing the breakwater elements to slide along the slope as well. A lower crest of the structure may result in the upper elements to be critical for damage, since the elements gain stability by the weight of the elements above.

In this paper, the main slope was seen to be rather stable, and relatively large irregularities seemed to be needed to significantly decrease the stability of the blocks. However, in the tests a straight slope with a high non-overtopped crest and with a fixed toe was considered. In realistic designs, the origin of failure is often located at these outer edges of the slope (toe and crest). Hence these items are a next item for further research. The toe could slide away, when an entire Xbloc$^{\text{Plus}}$layer can place force on the toe, as was observed for single layer cubes [Hofland and van Gent, 2016]. The upper rows are not stabilized by the weight of rows on top of them, so for lower-crested structures this might be the limiting factor for stability. The first application of the Xbloc$^{\text{Plus}}$ is the Afsluitdijk in the Netherlands, where 6.5 tonne units are placed. Here the blocks are used on the lower slope. Hence the highest element which is much less stable deserved extra attention [Janssen, 2018].

The Xbloc$^{\text{Plus}}$ units resemble other recently developed units like cubes that are placed in a single layer, the so-called C-ROC, and Seabees, as discussed in the introduction. These units can / are also placed in a regular fashion, they obtain their stability mainly from friction, and they are placed with such high density that pressures can build up underneath the layer. Therefore it is likely that these units have a similar tolerance for uneven placement as the presently studied unit. Hence when testing these types of units a similar procedure with irregular placement of the under layer could be followed. Moreover, the composition of the under layers is an important characteristic of the design, as the pressures under the armour layer during run down will be a function of the permeability of the under layer relative to that of the amour layer. Conversely, damage mechanisms that have been observed for other units (like the sliding of the toe due to the pressure of a single layer of cubes), might well be expected to be an important failure mechanism for the Xbloc$^{\text{Plus}}$.

The authors could not find much literature on the failure process of similar single layer units. Most knowledge is developed in-house at licence holders, and most findings seem to be reported in grey literature. Still we think it is important that these failure mechanisms of similar units should be reported, and based on the mechanisms that occur with other units. Hence, even though this paper is based on tests on one type of unit, the authors believe that the data and analyses presented might be relevant as it can serve as a reference point for the studies on other types of units. The development of the present units has been reported in various MSc theses at Delft University of Technology (repository.tudelft.nl).

9. Conclusions

In total 177 test runs have been performed on a breakwater slope with an armour consisting of regularly placed single layer interlocking units. Different types of irregularities in the underlayer were applied, that could potentially influence the interlocking of the elements. Based on these tests the following conclusions have been drawn.

It is possible to measure the size of the underlayer irregularities and the resulting orientation of breakwater elements by 3D reconstruction techniques based on photogrammetry. Additionally the measurement technique was able to indicate movements in the surface, which marks the initiation of damage.

Based on the results of the hydraulic model tests it can be concluded that the level of stability for single layer breakwater elements decreases when the size of the irregularities increases. An increase in the height of the irregularities causes the relative angle between neighbouring elements to increase which can lead to a loss of interlocking. Furthermore it increases the steepness of the slope at the lower side of the irregularity, such that the under layer becomes less resistant against being pushed outward.

The armour layer shows a maximum sensitivity to damage for convex deformations of the slope in the cross shore direction. A new failure mechanism for initiation of damage, not previously observed for breakwater elements, has been detected. This damage mechanism can occur when the armour layer is located on a protruding (convex) irregularity under the mean water line. During wave rundown the armour layer at this location is pushed outward by a combined effect of the weight of the upper armour and the hydraulic pressure of the remaining water under the top layer. The influence on the stability is quantified well by a linear formula that depends on the relative angle between the elements, caused by the radius of the irregularity, and the steepness of the lower slope. The latter has only been seen to be of influence in the case of macro irregularities and thus seems to be insignificant for micro irregularities. The steepness of the downward slope depends on both the actual distance between the top of the irregularity and the design profile, and the length scale of the irregularity.

The presently applied criteria for the placement of the underlayer for an Xbloc$^{\mathrm{Plus}}$ breakwater element is a maximum deviation from the design profile of 0.25 times D_n and a maximum deviation between succeeding measurements of 0.10 times D_n. These deviations from the design slope are small compared to the limiting value, such that the underlayer configuration will not influence the stability significantly.

References

Angremond, K., Van Roode, F.C., Verhagen, H., 2008. Breakwaters and closure dams. VSSD, Delft. 2nd edition.

Brouwer, M., 2013. The influence of the under layer on the stability of single layer armour units Master of Science Thesis. Master thesis. Delft University of Technology. Delft.

Burcharth, H., Andersen, O., 1995. On the One-Dimensional Unsteady Porous Flow Equation. Coastal Engineering 24, 233–257.

CUR, 1995. Design manual for pitched slope protection. . Klein Breteler for Ministry of Transport, Public Works and Water Management, Netherlands, Balkema, Rotterdam.

Dai, Y., Kamel, A., 1969. Scale effect tests for rubble-mound breakwaters: Hydraulic model investigation. Technical Report H-69-2. U.S. Army Engineer Waterways Experiment Station. Washington D.C.

De Almeida, E., Gent, M.V., Hofland, B., 2019. Damage Characterization of Rock Slopes. J. of Marine Science and Eng 7.

Docs.opencv.org, . OpenCV MatchTemplate documentation.

Garcia, N., Richardson, S., Rigden, T., 2013. Physical Model Testing of the Hydraulic Stability of Single-layer Armour Units, in: Coasts, Marine Structures and Breakwaters Conference, Institution of Civil Engineers, Edinburgh.

Hofland, B., van Gent, M., 2016. Automatic settlement analysis of single-layer armour layers, in: International Conference on the Application of Physical Modelling in Coastal and Port Engineering and Science, Coastlab, Ottawa.

Hudson, R.Y., 1959. Laboratory investigation of rubble-mound breakwaters. Technical Report. American Society of Civil Engineers. Vicksburg.

Jacobs, R., 2017. Internal memo; 2D Hydraulic Model Tests. Technical Report. Delta Marine Consultants. Gouda.

Janssen, D., 2018. Stability analysis of XblocPlus crest element. Master thesis. Delft University of Technology.

Loman, G., Hofland, B., van der Biezen, S., Poot, J., 2012. Integral design of hard sea defense of Maasvlakte 2, Part II: Physical model testing of cube revetment and reef, in: Coastlab12, Ghent University, Ghent.

Van der Meer, J., 1988. Stability of Cubes, Tetrapods and Accropode, in: Conference Breakwaters '88, Delft Hydraulics Laboratory, London. pp. 59–68.

ten Oever, E., Verhagen, H.J., Klabbers, M., Reedijk, B., 2012. Theoretical and experimental study on the placement of Xbloc armour units, in: International Conference on Coastal Engineering, American Society of Civil Engineers, San Diego.

Pardo, V., Herrera, M.P., Molines, J., Medina, J.R., 2013. Placement grids, porosity and randomness of armor layers. Waterway, Port, Coastal, and Ocean Engineering 140.

Perrin, S., Giraudel, C., Collinsworth, S., Melby, J., 2017. Hydraulic response & placement methods for a new single-layer concrete armour unit called C- ROC ™, in: Coasts, Marine Structures and Breakwaters Conference, Institution of Civil Engineers, Liverpool.

Rada Mora, B., 2017. Hydraulic performance of Xbloc+ armor unit. Master thesis. Delft University of Technology.

Van Gent, M., Luis, L., 2013. Application of cubes in a single layer, in: International Short Course/Conference on Applied Coastal Research, SCACR.

Vos, A.B., 2017. Exploration into the mechanisms that govern the stability of an Xbloc+ v1 armour unit. Master thesis. Delft University of Technology.

Van der Zwicht, B., 2015. Specifications of Application Xbloc. Technical Report. Delta Marine Consultants. Gouda.